

Nuclear Equation of State

Paweł Danielewicz

*National Superconducting Cyclotron Laboratory and Department of Physics and Astronomy,
Michigan State University, East Lansing, MI 48824, USA,
and Gesellschaft für Schwerionenforschung mbH, D-64291 Darmstadt, Germany*

Abstract. Nuclear equation of state plays an important role in the evolution of the Universe, in supernova explosions and, thus, in the production of heavy elements, and in stability of neutron stars. The equation constrains the two- and three-nucleon interactions and the quantum chromodynamics in nonperturbative regime. Despite the importance of the equation, though, its features had remained fairly obscure. The talk reviews new results on the equation of state from measurements of giant nuclear oscillations and from studies of particle emission in central collisions of heavy nuclei.

INTRODUCTION

An equation of state (EOS) is a nontrivial relation between thermodynamic variables characterizing a medium. While the term is used in its singular form in nuclear physics, actually different relations are of interest, such as between pressure p and baryon density ρ and temperature T , $p(\rho, T)$, or chemical potential μ and T , $p(\mu, T)$, between energy density e and ρ and T , $e(\rho, T)$, etc. Some of the relations are fundamental under certain conditions, i.e. all other relations may be derived from them (such as from $e(\rho)$ at $T = 0$).

The nuclear EOS is of interest because it affects the fate of the Universe at times $t \gtrsim 1 \mu\text{s}$ from the Big Bang and because its features are behind the supernova explosions. Moreover, its features ensure the stability of neutron stars. Through its effects on the evolution of the Universe, on supernovae explosions, and on neutron-star collisions, the EOS affects nucleosynthesis. Moreover, the EOS impacts central reactions of heavy nuclei. Finally, the form of the EOS constraints hadronic interactions and the nonperturbative quantum chromodynamics (QCD).

IMPORTANCE OF EOS

Different regimes for the strongly interacting are conveniently assessed in the $\mu - T$ plane, see Fig 1. Along the $T = 0$ axis, at $\mu \approx 930$ MeV, we have the matter in heavy nuclei. The matter in the interior of neutron stars corresponds to higher chemical potentials, in combinations with low temperatures. The matter in the early Universe evolved along the temperature axis, at low baryon number content, and thus at low μ . Different regions of the plane are explored at different accelerators. In the early Universe and likely at the higher-energy accelerators, the matter crosses the transition between the hadronic matter and quark-gluon plasma. The transition is observed in numerical lattice QCD calculations as a rapid change in energy density in the temperature region

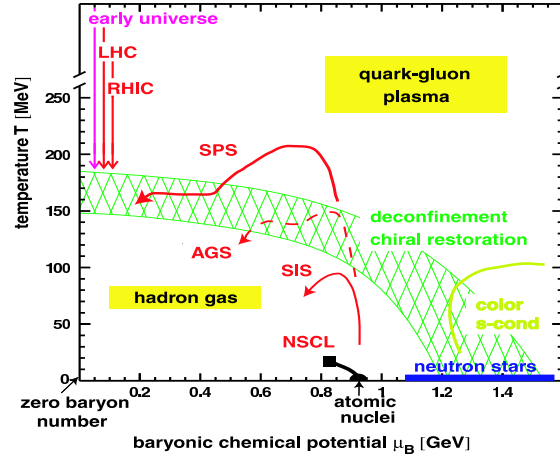


FIGURE 1. Strongly interacting matter in the $\mu - T$ plane, after [1]*.

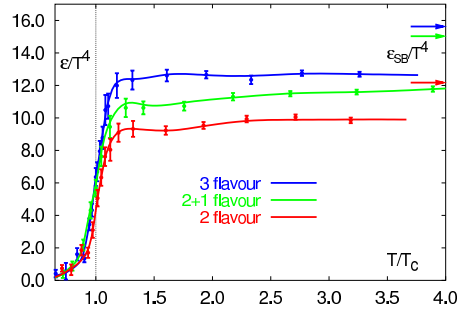


FIGURE 2. Energy in baryonless matter vs T , from calculations of Ref. [2].

of $T_c \sim 170$ MeV, cf. Fig. 2. The numerical calculations are carried out on a lattice of a finite size and it can be difficult to establish whether one deals just with a transitional behavior or with a phase transition and, if so, of what order. Whether or not there is a first-order phase transition is of importance for the early Universe.

Early Universe

Associated with a first-order phase transition is the surface tension σ and a possibility of supercooling. For sufficiently high σ , the early Universe might supercool down to temperatures as low as half of the critical temperature T_c , cf. Fig. 3. The large surface tension would lead to a wide separation, by as much as $\ell \sim 1$ m, of the forming hadronic bubbles and, eventually, as the hadronic bubbles grow and begin to fill all space, of the remnant quark-gluon bubbles, cf. Fig. 4. The separation would produce large nonuniformities, characterized by masses $M \sim 10^{18}$ kg (i.e. of a medium size asteroid), in the distribution of the baryon number following the hadronization, with the baryon number concentrated in the regions that hadronize last. The excess baryon number would get trapped in the quark-gluon bubbles, because the baryon number costs

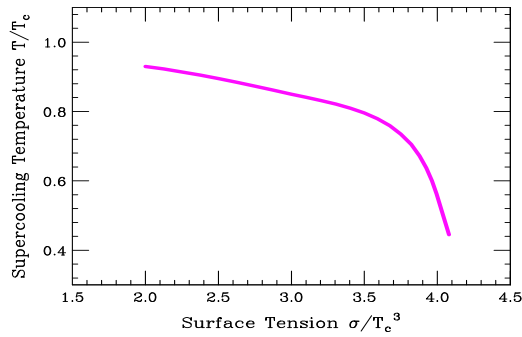


FIGURE 3. Supercooling tension for the confinement phase transition, after [3].

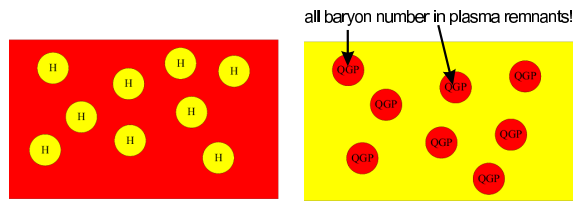


FIGURE 4. Phase bubbles in the region of the confinement phase transition, after [3].

little in the quark-gluon phase, with quarks being massless, and a lot in the hadronic phase, with massive baryons. An analogous situation takes place when seawater freezes. Then the salt appears in the areas that are last to freeze, Fig. 5. There are some cautioning theoretical and experimental indications, though, regarding the scenario, that the surface tension might not be very large between in the quark-gluon and hadron phases.

Supernova Explosions

Type II supernova explosions are the source of at least half of the nuclei heavier than iron around us. Only very massive stars, of masses $M \gtrsim 8M_{\odot}$, explode. Generally, the more massive a star, the shorter it lives, burning faster due to higher density and temperature in its interior. A star starts out burning hydrogen, then helium and successively heavier nuclei; at each stage the products are accumulated. After a given fuel runs out, the gravitation compresses the star core raising temperature and the next fuel ignites with its burning preventing further compression. When the core consists of iron only, the burning stops. It is then up to the electron pressure (such as resisting the compression of solids) to prevent the gravitational collapse of the core. However, the electron



FIGURE 5. Seawater analogy.

pressure fails when the core exceeds the threshold Chandrasekhar mass. This is seen by examining the contributions to the energy from gravity and from an ultrarelativistic electron gas:

$$\begin{aligned}
 E &= -\frac{3}{5}G\frac{(Nm_N)^2}{R} + N_e\left(\frac{3}{4}p_{Fc} + \frac{3m_e^2c^4}{2p_{Fc}} + \dots\right) + \dots \\
 &= \frac{1}{R}\left(-\frac{3}{5}G(Nm_N)^2 + \frac{3}{4}\hbar c\left(\frac{9\pi}{4}\right)^{1/3}N_e^{4/3}\right) + O(R). \tag{1}
 \end{aligned}$$

The electron Fermi momentum is proportional to the cube root of electron density and, thus, is inversely proportional to core radius, $p_F \propto \rho_e^{1/3} \propto 1/R$. Both the gravitational and electron energies are then inversely proportional to the radius, but the electron energy grows only as the number of electrons to the 4/3 power while the gravitational energy as the square power of the nucleon number. For the electron number equal to half the nucleon number, $N_e = N_N/2$, the gravity wins over electrons for core mass

$$M > M_{th} = \left(\frac{5\hbar c}{6G}\right)^{3/2} \frac{3\pi^{1/2}}{m_N^2} \sim 1.5M_\odot. \tag{2}$$

When the iron core exceeds the threshold mass, a gravitational collapse of the core starts and progresses till the nuclear densities are reached. The nuclear matter is more incompressible than the electron gas – what starts as an implosion gets reversed at the nuclear densities into an explosion. From the center of star a shock wave moves out, see the schematic view in Fig. 6, while at the center a so-called protoneutron star forms at a density of the order of that in nuclei. Inside, as the electron Fermi energy exceeds the proton-neutron mass difference, the process of neutronization takes place, $e^- + p \rightarrow \nu_e + n$. Additionally, thermal neutrinos are copiously produced. In the meantime, the shock moving through the infalling material stalls outside of the protostar and gets, most likely, revived by the neutrinos coming out from the center. Aside from propelling the shock, the neutrinos drive the neutron wind from the center within which copper, nickel, zinc and other elements form. Eventually, the shock reaches the star surface producing a magnificent display in the sky and throwing $7M_\odot$ of material space. The properties of nuclear matter, where the collapse reverses and that is the site of neutrino production, are, however, generally not well known.

Neutron Stars

The protoneutron star eventually turns into a black hole or into a neutron star. Which is the case depends on the properties of nuclear matter, Fig. 7. Dependent on those properties are also the characteristics of the forming neutron star and, in particular, the density profile and radius, see Fig. 8. In astrophysical modelling of neutron stars or of supernova explosions, a host of nuclear EOS is employed, such as those in Fig. 9, in terms of the dependence on pressure on energy density. Some EOS are excluded by causality (those with high p) and some by known masses of existing neutron stars (those

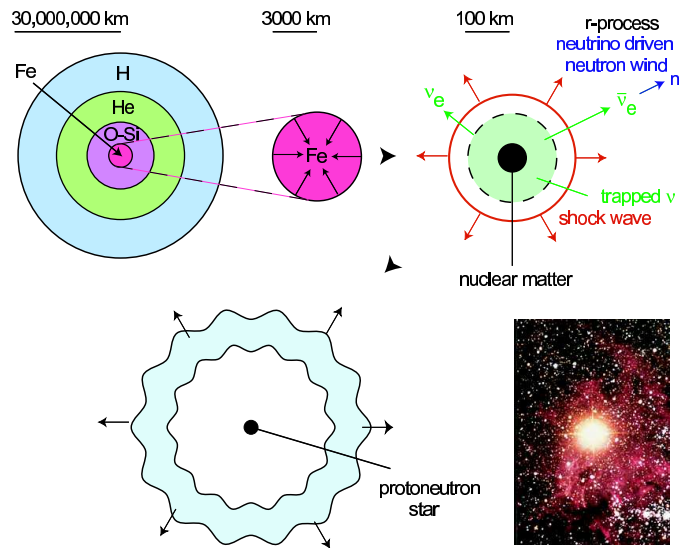


FIGURE 6. Supernova explosion.

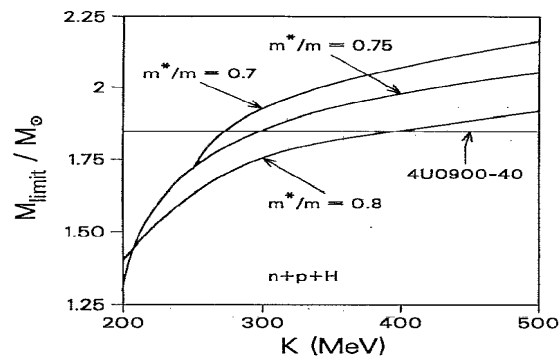


FIGURE 7. Limiting neutron star mass as a function of the compression modulus of the corresponding symmetric matter [5]*.

with low p). This still leaves a wide range of possibilities; there are EOS taken from nonrelativistic and relativistic calculations and some of the EOS incorporate different types of phase transitions.

A possible site for the synthesis of heavy elements, other than supernova explosions, are mergers of neutron stars. These mergers shed much more matter into space if the nuclear EOS is relatively soft than when it is stiff, Fig. 10.

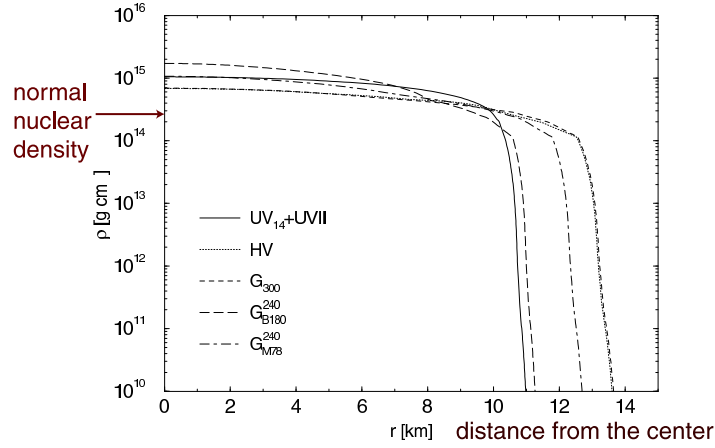


FIGURE 8. Density profile of a neutron star of mass $M = 1.4M_{\odot}$, after [4].

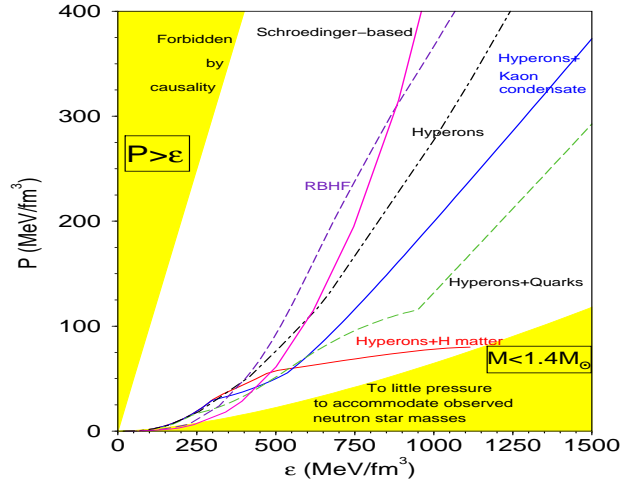


FIGURE 9. Pressure-energy relations [6] for nuclear matter, employed in astrophysical calculations.

ELEMENTARY FEATURES OF THE NUCLEAR EOS

Energy Minimum

The advances in the determination of the nuclear EOS have been, generally, difficult. The elementary information comes from the Weizsäcker binding-energy formula and from the systematics of nuclear density profiles. The Weizsäcker formula separates out the contributions to the energy associated with nuclear interactions and the interior and surface of nuclei, the contributions associated with isospin asymmetry and with Coulomb interactions, and the shell correction,

$$\begin{aligned}
 -B(A, Z) = & -16\text{MeV}A + a_s A^{2/3} \\
 & + a_a \frac{(A - 2Z)^2}{A} + a_c \frac{Z(Z - 1)}{A^{1/3}} - B_{p,s}. \quad (3)
 \end{aligned}$$

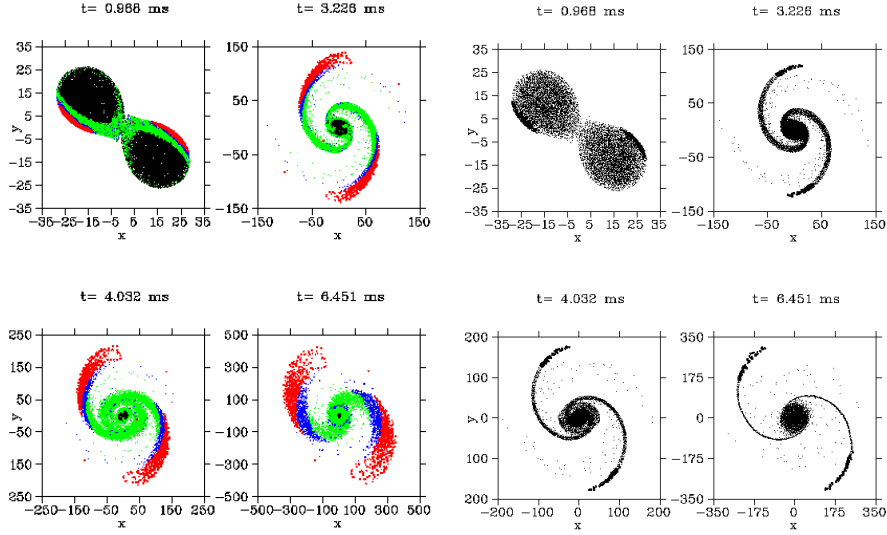


FIGURE 10. Neutron star mergers for soft (left panels) and stiff (right panels) nuclear EOS, after [7].

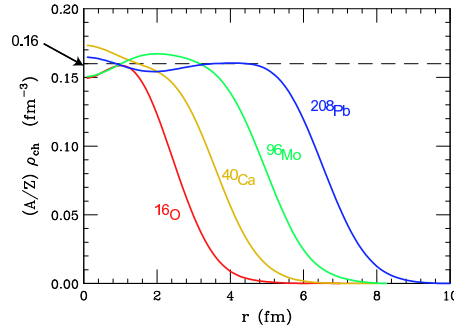


FIGURE 11. Nuclear densities deduced from electron scattering.

Nuclear densities, obtained from charge densities multiplied by mass to charge number ratio, are seen to reach the same value, $\rho_0 = 0.16 \text{ fm}^{-3} \simeq 1/(6 \text{ fm}^3)$, for a wide range of nuclear masses, see Fig. 11. We conclude that the energy per nucleon in a uniform symmetric nuclear matter at $T = 0$, in the absence of Coulomb interactions, has a minimum at the normal density ρ_0 with the energy value, relative to nucleon mass, of -16 MeV , from the volume term in the binding formula, see Fig. 12. As, obviously, the binding energy approaches zero for separated nucleons at $\rho \rightarrow 0$, we actually know two points in the ($T = 0$) dependence of the energy per nucleon, $E/A \equiv e/\rho$, on density.

The next nontrivial feature of the energy per nucleon is its curvature in the dependence on ρ , around ρ_0 . This curvature is commonly quantified in terms of the so-called nuclear incompressibility, with an unusual numerical factor:

$$K = 9\rho_0^2 \frac{d^2}{d\rho^2} \left(\frac{E}{A} \right) = R^2 \frac{d^2}{dR^2} \left(\frac{E}{A} \right). \quad (4)$$

The factor stems from the fact that the nuclei were first considered as sharp-edged

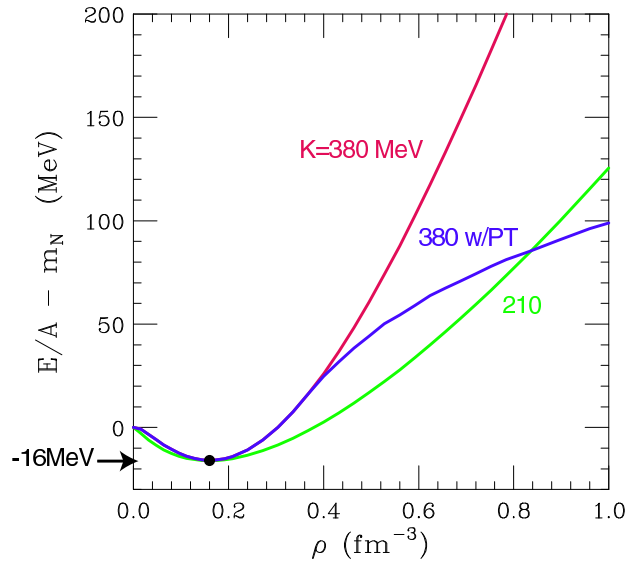


FIGURE 12. Energy per nucleon vs density in nuclear matter.

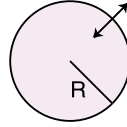


FIGURE 13. Oscillating nuclei were first considered as sharp-edged spheres with the energy changing as a function of the radius.

spheres with the energy changing as a function of the radius (Fig. 13). To get an idea of what might be expected for the incompressibility, one might just run a parabola through the two known points on the curve of $\frac{E}{A}(\rho)$. The then resulting incompressibility has a value of $K \sim 290$ MeV. If the actual incompressibility turns out to be below this benchmark value, we may consider the nuclear EOS to be soft, and stiff if the opposite is the case.

Microscopic Calculations

To get the features of the nuclear EOS outside of the minimum, one might turn to microscopic calculations, such as within Brueckner and variational frameworks. These calculations utilize elementary nucleon-nucleon interactions constrained by nucleon-nucleon interactions and by deuteron properties. However, the nonrelativistic calculations with only nucleon-nucleon interaction miss the known position of the minimum in the nuclear EOS; the minima line up along the so-called Coester line (Fig. 14) in the energy vs density or Fermi momentum, with the change of the version of the interaction. The relativistic calculations line up along another Coester line that passes closer to the true minimum; aside from relativity, though, those calculations are generally more

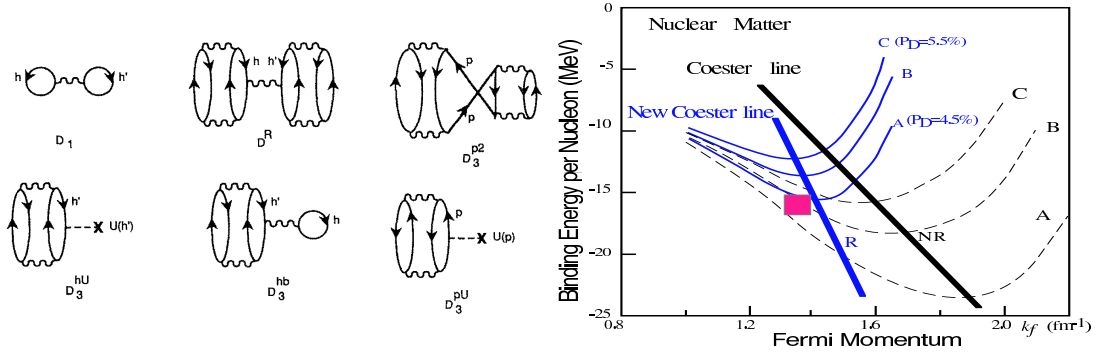


FIGURE 14. Left: Diagrams for different terms in the energy per nucleon in many-body calculations [8]. Right: Binding energy vs Fermi momentum in many-body calculations, after [9].

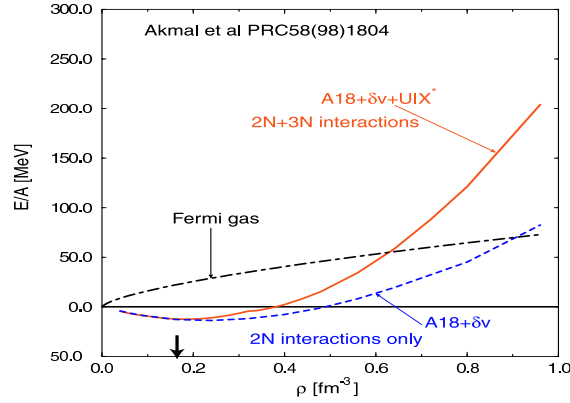


FIGURE 15. Energy per nucleon in nuclear matter as a function of density, from a variational calculation of Ref. [10] with two- and three-nucleon interactions.

primitive than the nonrelativistic ones.

To get the right position of the minimum in the EOS, Fig. 15, it is necessary to incorporate three-nucleon interactions in the microscopic calculations. These interactions are not well constrained by scattering, hampering the predictive power of the theory. In this situation, one may want to turn to experiment to get the information on the EOS away from the normal density.

INCOMPRESSIBILITY - GETTING OUT OF THE MINIMUM

The simplest way to determine the incompressibility experimentally may seem to induce volume oscillations in a nucleus. This could be done by scattering α particles off a nucleus, Fig. 16. For the lowest excitation, the excitation energy E^* , deduced from the final α energy, would be related to the classical frequency through $E^* = \hbar\Omega$, and the latter would be related to K . Let us examine the classical energy of an oscillating nucleus:

$$E_{tot} = \int d\mathbf{r} \rho \frac{m_N v^2}{2} + \frac{1}{2} A K (R - R_0)^2$$

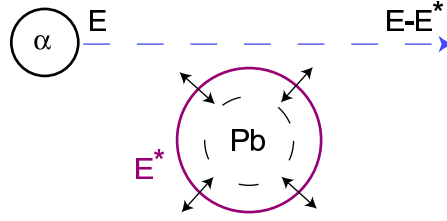


FIGURE 16. Volume oscillations induced by alpha scattering.

$$= \frac{Am_N \langle r^2 \rangle_A \dot{R}^2}{2} + \frac{1}{2} AK(R - R_0)^2, \quad (5)$$

where we use the fact that, for a nucleus uniformly changing its density, the velocity is proportional to the radius, $v = \dot{R}(r/R)$. We then obtain the energy of a simple harmonic oscillator; the frequency is a square root of the spring constant divided by mass constant, yielding:

$$E^* = \hbar \sqrt{\frac{K}{m_N \langle r^2 \rangle_A}}. \quad (6)$$

There are complications regarding this reasoning. Thus, the nucleus is not a sharp-edged sphere and the Coulomb interactions play a role in the oscillations as well as nuclear interactions. These effects may be taken care of by using an incompressibility constant characteristic for a nucleus, $K \rightarrow K_A$, and isolating different contributions in an analogy to those for the binding energy:

$$K_A = K + K_s A^{-1/3} + K_a \left(\frac{N-Z}{A} \right)^2 + K_c \frac{Z(Z-1)}{A^{4/3}} + \dots \quad (7)$$

With the corrections, it turns out that the incompressibilities for medium to heavy nuclei are about 2/3 of the incompressibility for infinite nuclear matter, e.g. $K^{Pb} \sim 0.64K$; $K^{Sm} \simeq 0.67K$.

However, there are more problems. Thus, the density oscillations lie high up in the excitation energy and get broadened up. This may be remedied by employing a sum rule (notably, sum rules are often robust tools in helping to link simple classical considerations with the characteristics of quantum states):

$$\hbar \sqrt{\frac{K_A}{m_N \langle r^2 \rangle_A}} = \sqrt{\frac{\langle E^{*3} \rangle_{0+ \text{ spectrum}}}{\langle E^* \rangle_{0+ \text{ spectrum}}}}, \quad (8)$$

i.e. the incompressibility may be obtained from dividing the third by the first moment of the spectrum. An alternative is to use a microscopic theory, with an effective interaction, to describe both the excitation spectrum and the incompressibility for infinite matter.

The final complication is that other types of oscillations, than that changing the density, are excited in scattering, such as the oscillation of protons vs neutrons and

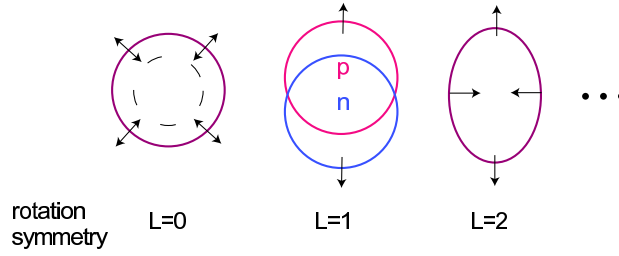


FIGURE 17. Different collective oscillations transform differently under rotations.

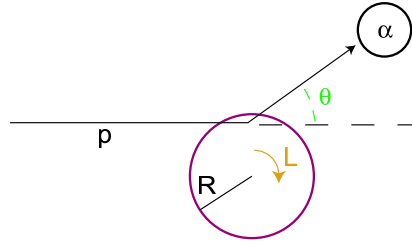


FIGURE 18. Delivering angular momentum to a target.

the quadrupole shape oscillation, cf. Fig. 17. However, those oscillations transform differently under rotations and, correspondingly, the elementary excitations for those oscillations are characterized by different angular momenta, with the uniform density changes characterized by $L = 0$. It is possible to isolate the $L = 0$ excitations by analyzing scattering at the very forward angles, Fig. 18. When the alpha particle scatters off a nucleus it transfers linear and angular momenta to the nucleus. The angular momentum is limited by the product of the linear momentum transfer and the distance over which the transfer occurs, i.e. roughly the sum of projectile and target radii. At high beam energies and small angles we get

$$L < |p - p'|R \approx p\theta R. \quad (9)$$

Excitations characterized by $L \geq 1\hbar$ may be suppressed by looking at scattering into the angles $\theta < \frac{\hbar}{pR}$, i.e. within the first diffraction peak.

Scattering of alpha particles from different targets has been carefully studied in recent years simultaneously as a function of excitation energy and scattering angle, allowing to isolate the contributions of $L = 0$ excitations [11, 12], see Fig. 19 for data from a samarium target. For the shown excitation energy of 16.5 MeV, a pronounced $L = 0$ peak is evident at low scattering angles. The $L = 0$ excitation strength is next shown for the samarium target in Fig. 20. A peak is evident at the excitation energy of 15.5 MeV, yielding an incompressibility of samarium $K^{Sm} = \frac{E^{*2}m_N \langle r^2 \rangle_A}{\hbar^2} = 138 \text{ MeV}$, and of nuclear matter $K = K^{Sm}/0.67 \sim 210 \text{ MeV}$. However, explorations with microscopic models produce different results for K_A/K . In particular, relativistic models can yield results in the range $K \sim (250 - 270) \text{ MeV}$ [13]. Generally, the results are, though, on the soft side of the incompressibility.

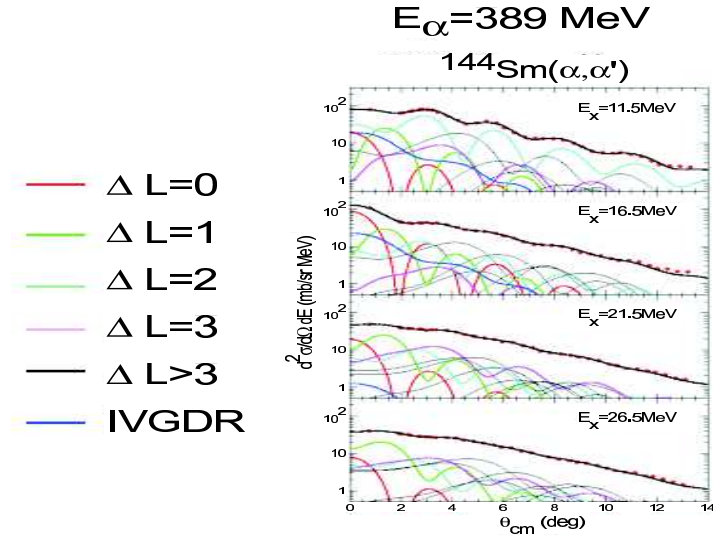


FIGURE 19. Alpha scattering cross section from ^{144}Sm , determined in Ref. [12].

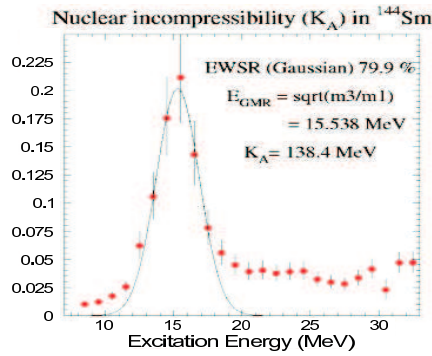


FIGURE 20. 0^+ -strength function in ^{144}Sm , determined in Ref. [12].

EOS AT SUPRANORMAL DENSITIES FROM FLOW

Features of EOS at supranormal densities can be inferred from flow produced in collisions of heavy nuclei at high energies. At low impact parameters, in those collisions, macroscopic regions of high density are formed. The collective flow, that can be quantitatively assessed in collisions, is the particle motion characterized by space-momentum correlations of dynamic origin. The flow can provide information on the pressure generated in the collision.

To see how the flow relates to pressure, we may look at the hydrodynamic Euler equation for the nuclear fluid, an analog of the Newton equation, in a local frame where the collective velocity vanishes, $v = 0$:

$$(e + p) \frac{\partial}{\partial t} \vec{v} = -\vec{\nabla} p. \quad (10)$$

The collective velocity becomes an observable at the end of the reaction. In comparing

to the Newton equation, we see that the pressure $p = \rho^2 \frac{\partial(e/\rho)}{\partial \rho} |_{s/\rho}$ plays the role of a potential for the hydrodynamic motion, while the density of enthalpy $w = e + p$ plays the role of a mass. In fact, at moderate energies, the enthalpy density is practically the mass density, $w \approx \rho m_N$. We see from the Euler equation that the collective flow can tell us about the pressure in comparison to enthalpy. In establishing the relation, we need to know the spatial size where the pressure gradients develop and this will be determined by the nuclear size. However, we also need the time during the hydrodynamic motion develops and this can represent a problem.

The equilibrium required for hydrodynamics is not quite achieved in reactions and, thus, transport theory is actually required to establish links between the EOS and observables; the hydrodynamics just yields important insights. The reacting system in the transport theory relying on Boltzmann equation is described in terms of the phase-space distribution functions f for different particles. In particular, the system energy is a functional of the distributions, $E\{f\}$, and can be parametrized to yield different EOS in equilibrium. The distributions follow a set of the Boltzmann equations with single-particle energies that are functional derivatives of the energy, $\varepsilon = \delta E / \delta f$:

$$\frac{\partial f}{\partial t} + \frac{\partial \varepsilon}{\partial \mathbf{p}} \frac{\partial f}{\partial \mathbf{r}} - \frac{\partial \varepsilon}{\partial \mathbf{r}} \frac{\partial f}{\partial \mathbf{p}} = I, \quad (11)$$

where I is the collision integral.

The first observable that one may want to consider to extract the information on EOS is the net radial or transverse collective energy. That energy may reach as much as half of the total kinetic energy in a reaction. Despite its magnitude, the energy is not useful for extracting the information on EOS because of the lack of information on how long the energy develops. Large pressures acting over a short time can produce the same net collective energy as low pressures acting over a long time. This makes apparent the need for a timer in reactions.

The role of the timer in reactions may be taken on by the so-called spectators. The spectator nucleons are those in the periphery of an energetic reaction, weakly affected by the reaction process, proceeding virtually at undisturbed original velocity, see Fig. 21. Participant nucleons, on the other hand, are those closer to the center of the reaction, participating in violent processes, subject to matter compression and expansion in the reaction. As the participant zone expands, the spectators, moving at a prescribed pace, shadow the expansion. If the pressures in the central region are high and the expansion is rapid, the anisotropies generated by the presence of spectators are going to be strong. On the other hand, if the pressures are low and, correspondingly, the expansion of the matter is slow, the shadows left by spectators will not be very pronounced.

There are different types of anisotropies in the emission that the spectators can produce. Thus, throughout the early stages of a collisions, the particles move primarily along the beam axis in the center of mass. However, during the compression stage, the participants get locked within a channel, tilted at an angle, between the spectator pieces, cf. Fig. 21. As a consequence, the forward and backward emitted particles acquire an average deflection away from the beam axis, towards the channel direction. Another anisotropy may be observed for particles emitted in the transverse directions with zero longitudinal velocity. The region with compressed matter is open to the vacuum in

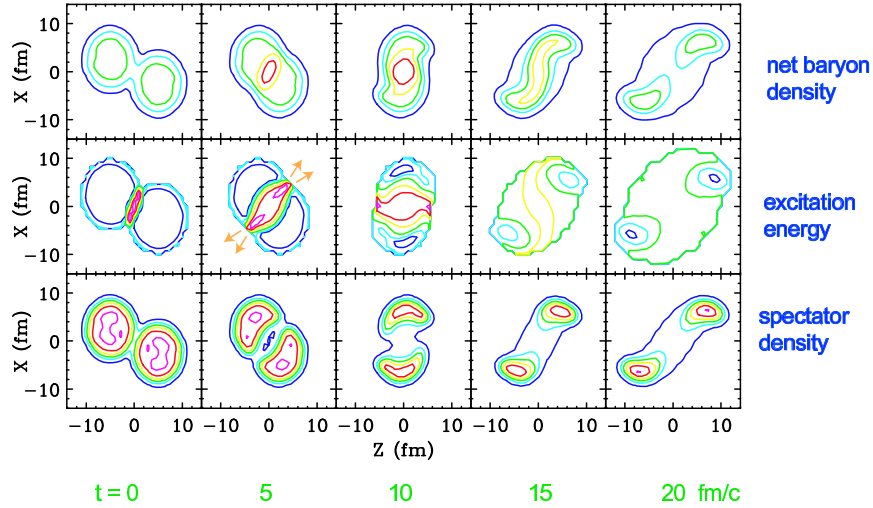


FIGURE 21. Reaction-plane contour plots for different quantities in a $^{124}\text{Sn} + ^{124}\text{Sn}$ reaction at 800 MeV/nucleon and $b = 6$ fm, from transport simulations by Shi [14].

the direction perpendicular to the reaction plane. However, in the direction within the reaction plane the region is shadowed by the participants. Thus, more particles are expected to be transversally emitted from the participant region perpendicular than within the direction plane. The anisotropy should be stronger the faster the expansion of the compressed matter.

The different anisotropies have been quantified experimentally over a wide range of bombarding energies. Figure 22 shows the measure of the sideward forward-backward deflection in Au + Au collisions as a function of the beam energy, with symbols representing data. Lines represent simulations assuming different EOS. On top of the figure, typical maximal densities are indicated which are reached at a given bombarding energy. Without interaction contributions to pressure, the simulations labelled cascade produce far too weak anisotropies to be compatible with data. The simulations with EOS characterized by the incompressibility $K = 167$ MeV yield adequate anisotropy at lower beam energies, but too low at higher energies. On the other hand, with the EOS characterized by $K = 380$ MeV, the anisotropy appears too high at virtually all energies. It should be mentioned that the incompressibilities should be considered here as merely labels for the different utilized EOS. The pressures resulting in the expansion are produced at densities significantly higher than normal and, in fact, changing in the course of the reaction.

Figure 23 shows next the anisotropy of emission at midrapidity or zero longitudinal velocity in the c.m., cf. Fig. 24, with symbols representing data and lines representing simulations. Again, we see that without interaction contributions to pressure, simulations cannot reproduce the measurements. The simulations with $K = 167$ MeV give too little pressure at high energies, and those with $K = 380$ MeV generally too much. A level of discrepancy is seen between data from different experiments.

We see that no single EOS allows for a simultaneous description of both types of anisotropies at all energies. In particular, the $K = 210$ MeV EOS is best for the sideward anisotropy, and the $K = 300$ MeV EOS is the best for the other, so-called

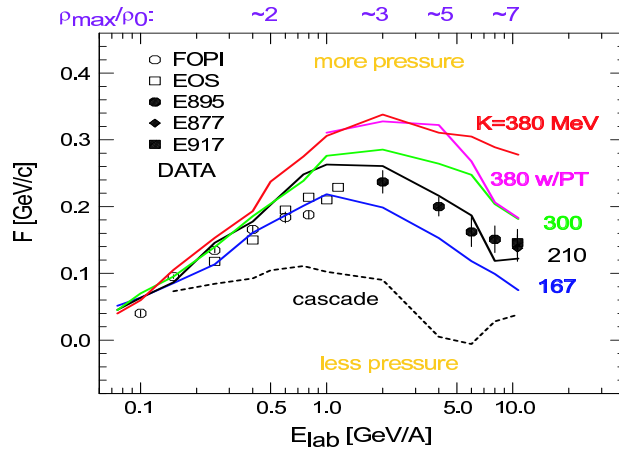


FIGURE 22. Sideward flow excitation function for Au + Au. Data and transport calculations are represented, respectively, by symbols and lines [15].

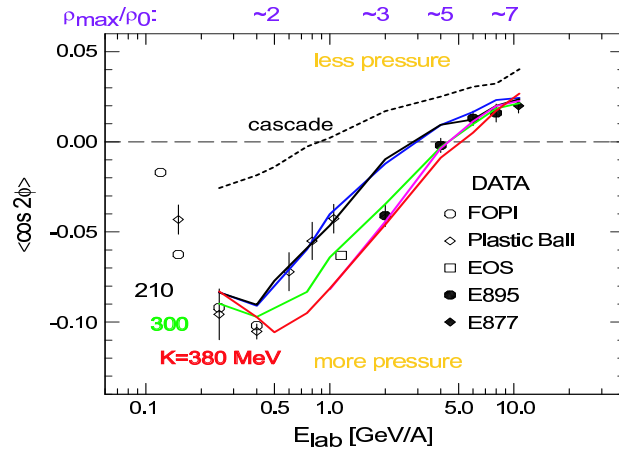


FIGURE 23. Elliptic flow excitation function for Au + Au. Data and transport calculations are represented, respectively, by symbols and lines [15].

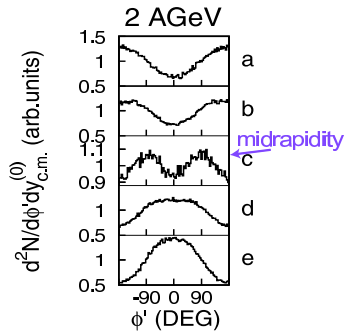


FIGURE 24. Azimuthal distribution of protons from Au + Au collisions at 2 GeV/nucleon in different rapidity intervals [16].

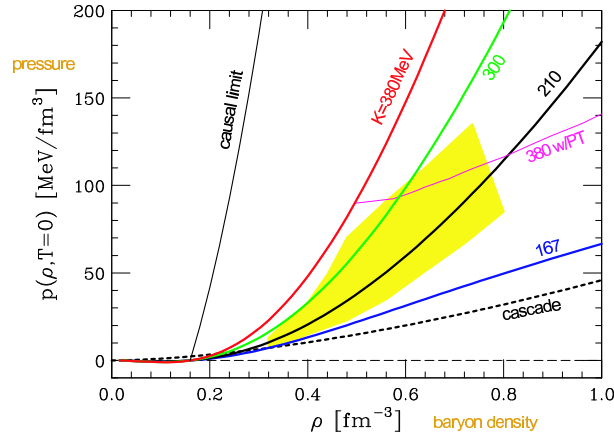


FIGURE 25. Constraints from flow on the $T = 0$ pressure-density relation, indicated by the shaded region [15].

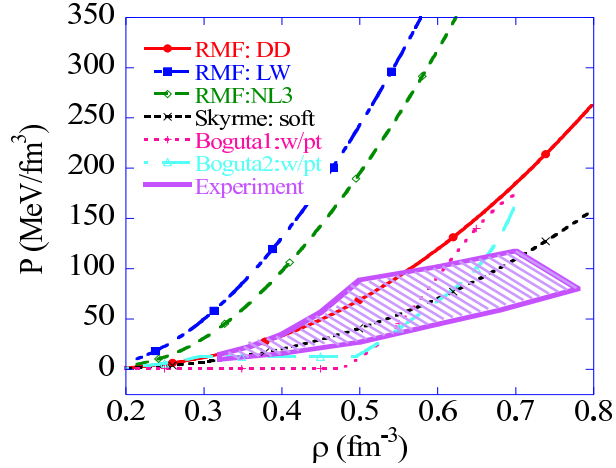


FIGURE 26. Impact of the constraints on models for EOS [15].

elliptic, anisotropy. We can use the discrepancy between the conclusions drawn from the two types of anisotropies as a measure of inaccuracy of the theory and draw broad boundaries on pressure as a function of density from what is common in conclusions based on the two anisotropies. To ensure that the effects of compression dominate in the reaction over other effects, we limit ourselves to densities higher than twice the normal. The boundaries on the pressure are shown in Fig. 25 and they eliminate some of the more extreme models for EOS utilized in nuclear physics, such as the relativistic NL3 model and models assuming a phase transition at relatively low densities, cf. Fig. 26.

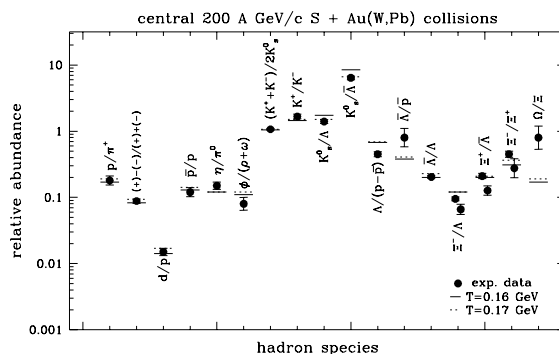


FIGURE 27. Relative particle abundancies in measurements (symbols) and calculated in the thermal freeze-out model (lines) in Ref. [17].

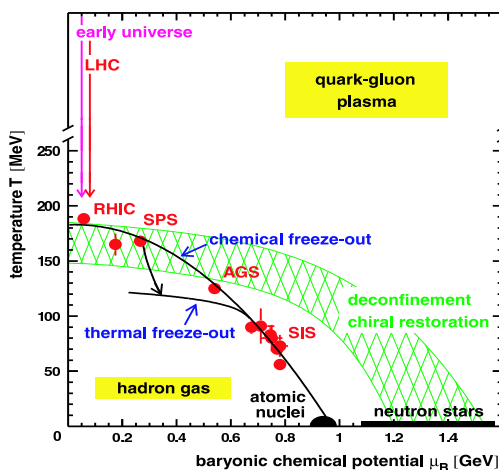


FIGURE 28. Freeze-out temperature and baryon chemical potential*.

HIGH- T LOW- ρ LIMITS OF THE HADRONIC WORLD

In central reactions of medium to heavy nuclei, over a broad range of bombarding energies, it is found that hadronic yields are consistent with thermal equilibrium at definite T and μ when interactions appear to stop [17, 18]. This is illustrated in Fig. 27 showing measured particle yields and those calculated assuming thermal equilibrium. The results indicate that, at the deduced temperatures and chemical potentials, the spectrum of hadrons is close to that in free space and, thus, the phase transition to quark-gluon phase has not been crossed. The boundaries of the hadronic world, staked out in this fashion, are shown in Fig. 28.

CONCLUSIONS AND OUTLOOK

Nuclear EOS ties together different areas of physics. Progress on the EOS has been made in different directions. Data on giant monopole resonances (and also on giant

vector resonances) have been collected with significant background reductions and high resolution both in the energy and angle direction, allowing for improved determinations of the nuclear incompressibility. Anisotropies of flow from central reactions allow to constrain the EOS at supranormal densities. The parameters of freeze-out in reactions allow to stake out the limits of the hadronic world. Additional sources of information on EOS that I had no chance to talk about include measurements of neutron-star properties, studies of nuclear systematics and lattice QCD calculations. Unconquered EOS frontiers include the dependence of EOS on the isospin degree of freedom and the detection of the quark-gluon plasma. The first frontier is, in particular, to be tackled at the NSCL coupled-cyclotrons and at the proposed RIA accelerator. In the baryonless regime, the second frontier is pursued at RHIC. However, the baryon-rich regime awaits stepped-up dedicated studies with good resolution in bombarding energy in the range of (2-40) GeV/nucleon.

ACKNOWLEDGMENTS

Information provided by M. Itoh on giant resonances is gratefully acknowledged. This work was partially supported by the National Science Foundation under Grant PHY-0070818.

*Original figures from Refs. [1] and [4], respectively, have been utilized, with permission from Elsevier Science.

REFERENCES

1. J. Stachel, Nucl. Phys. A654, 119c (1999).
2. F. Karsch, hep-lat/0106019.
3. B. Kämpfer *et al.*, nucl-th/0011088.
4. Ch. Schaab *et al.*, Nucl. Phys. A605, 531 (1996).
5. N. K. Glendenning, Phys. Rev. C 37, 2733 (1988).
6. F. Weber, *Pulsars as Astrophysical Laboratories for Nuclear and Particle Physics*, IoP Publishing, Bristol (1999).
7. S. Rosswog *et al.*, Astronomy and Astrophysics 341, 499 (1999).
8. M. Baldo *et al.*, Phys. Rev. C 41, 1748 (1990).
9. R. Brockmann and R. Machleit, Phys. Rev. C 42, 1965 (1990).
10. A. Akmal, V. R. Pandharipande, and D. G. Ravenhall, Phys. Rev. C 58, 1804 (1998).
11. D. H. Youngblood, Nucl. Phys. A687 1c (2001).
12. M. Itoh *et al.*, Nucl. Phys. A687, 52c (2001).
13. D. Vretenar *et al.*, Nucl. Phys. A621, 853 (1997).
14. L. Shi, P. Danielewicz and R. Lacey, Phys. Rev. C 64, 034601 (2001).
15. P. Danielewicz, W. Lynch and R. Lacey (2001), to be published.
16. C. Pinkenburg *et al.*, Phys. Rev. Lett. 83, 1295 (1999).
17. P. Braun-Munzinger *et al.*, Phys. Lett. B 365, 1 (1996).
18. J. Cleymans and K. Redlich, Nucl. Phys. A661, 379c (1999).